

Influence of Induction and Furnace Postweld Heat Treatment on Corrosion Properties of SAF 2205 (UNS 31803)

When postweld heat treatment of duplex stainless steels is prescribed, accurate control of time and temperature across the entire thickness of the bead is necessary to guarantee good corrosion properties

P. FERRO, A. TIZIANI, AND F. BONOLLO

ABSTRACT. The duplex stainless steels are well known for their excellent combination of strength and corrosion resistance, which is strictly related to control of the composition and the microstructural balance. When duplex stainless steels are welded, the thermal cycles and rapid cooling caused by the welding process may alter the original microstructure, thereby affecting the above-mentioned properties of the base material. However, if welding is accomplished by using specific filler metals for duplex steels, the application of a postweld heat treatment on duplex stainless steels is usually not needed. Nevertheless, for certain applications it is prescribed by technical standards to submit the workpiece to solution heat treatment or stress-relieving annealing before use. The heat treatment of duplex stainless steels requires very accurate control of both time and temperature.

In this work, the influence of postweld heat treatments on the corrosion resistance of a duplex stainless steel (SAF 2205, alias UNS 31803) has been analyzed. Different results may be obtained if furnace heat treatment is used instead of an induction one. Thus, the study was specifically aimed at a detailed investigation of the corrosion behavior of welded components after induction postweld heat treatment and furnace postweld heat treatment. It was found that pitting corrosion resistance is affected by the presence of secondary austenite and its morphology. Such morphology depends on time and temperature parameters so that if postweld induction heat treatment is used, the temperature gradient across the thickness of the joint has to be taken into account.

P. FERRO (ferro@gest.unipd.it), A. TIZIANI, and F. BONOLLO are with Department of Management and Engineering, University of Padova, Vicenza, Italy.

Introduction

It is well known that welding operations modify the ferrite/austenite phase balance (1:1) in duplex stainless steels (DSSs) and could promote the intermediate-phases precipitation in the weld metal and heat-affected zone (HAZ) (Refs. 1–5). The main consequence of this phenomenon is that corrosion resistance and mechanical properties of these materials are dramatically affected.

Since it would not be practical to postweld heat treat or hot work the large weldments, it is necessary to use a filler metal that can provide an as-deposited balanced microstructure. For this reason, recommended filler metals for the duplex stainless steels are of matching compositions except that nickel is increased to 8–10%.

However, American and European standards (ASTM A928/A928M and NORSOK MDS D42 standards, for example, Ref. 6) require the application of a postweld heat treatment (PWHT). In particular, these specifications cover standard requirements for ferritic/austenitic (duplex) stainless steel pipe that is electric fusion welded with the addition of filler metal suitable for corrosive service. Heat treatment shall be performed after welding and in accordance with specified temperature and quench conditions.

In order to properly balance the mi-

crostructure, any heat treatment of a duplex stainless steel should consist of a full solution annealing, meeting the minimum temperatures specified for the mill product in the ASTM specifications, followed by water quenching. In the case of the investigated steel, the UNS 31803 (also known by the commercial name SAF 2205), the minimum annealing temperature is 1040°C.

When there is a full solution anneal and quench subsequent to welding, that heat treatment is a part of the welding procedure. Possible applications can be found in the chemical and petrochemical industries, refineries, and gas and hydrocarbon transport. In addition, some types of equipment manufactured from duplex stainless steel require a full anneal. For example, the forming of large heads or the fabrication of some valve and pipe assemblies may require annealing. Annealing can restore the equilibrium phase balance and eliminate the problems associated with excessive ferrite and intermetallic phases. Such intermetallic phases are very dangerous for the mechanical and corrosion resistance of the joint and the risk of their precipitation may increase in the case of multipass welding.

Young et al. (Ref. 7) studied the effect of postweld heat treatment at 1050°C on UNS S31803. They obtained a good balance of ferrite/austenite after 15 min, while the best results were reached after 30 min. Melotti et al. (Ref. 8) studied the solution heat treatment of different duplex stainless steels. The lowest solubilization temperature (1050°C) was determined by the request to solubilize secondary phases precipitated after prior heat treatments while the higher solubilization temperature (1100°C) was determined by the request to keep δ/γ phase balance. Moreover, they found that for

KEYWORDS

Duplex Stainless Steels
Pitting Corrosion Resistance
Secondary Austenite
Postweld Heat Treatment

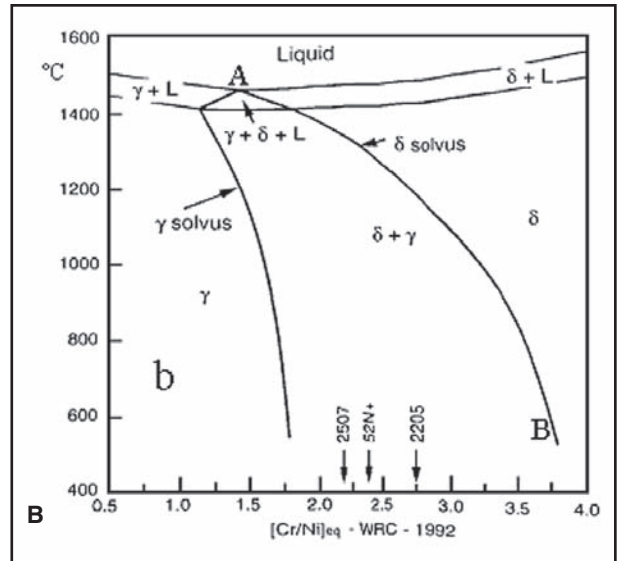
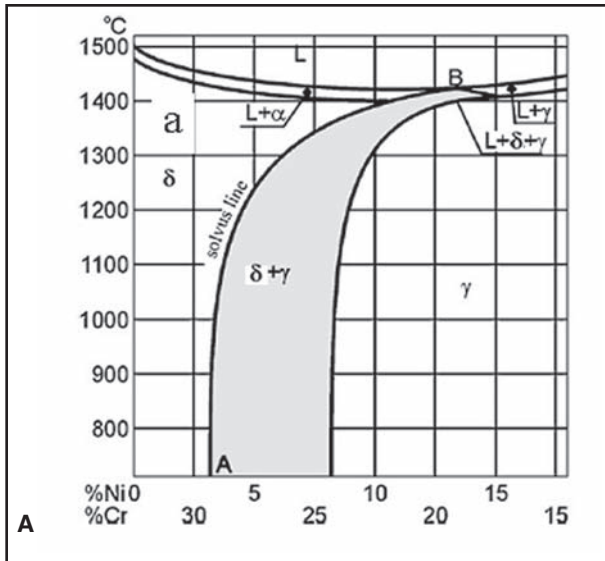


Fig. 1 — A — Fe-Cr-Ni equilibrium system for 68% Fe; B — WRC diagram related to DSS and SDSS (superduplex stainless steels) (Ref. 3).

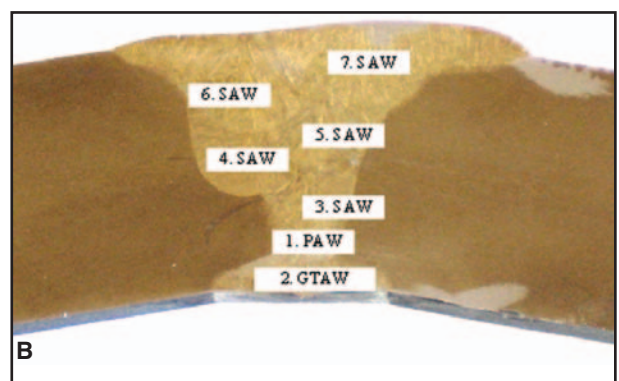
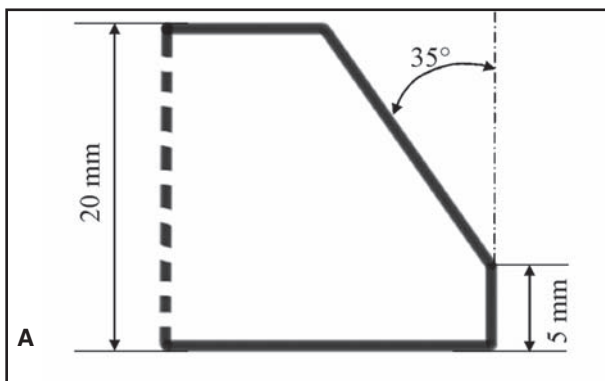


Fig. 2 — Welding configurations. A — Schematic representation of the adopted groove; B — weld run sequences.

duplex stainless steels with low chromium content the critical cooling rate, necessary to avoid intermediate phases, is about 0.3°C/s, while for higher chromium and molybdenum contents it is about 1°C/s.

In various works (Refs. 9–11), it was shown that the corrosion resistance of duplex stainless steels is also influenced by secondary austenite γ_2 -precipitation. This phase is formed as a result of the $\delta + \gamma \rightarrow \delta + \gamma + \gamma_2$ transformation in the austenitic-ferritic structure, following the heating to temperature below the A-B line in the phase equilibrium diagram of Fe-Cr-Ni in Fig. 1A. The secondary austenite may emerge as a result of an eutectoid transformation ($\delta \rightarrow \sigma + \gamma_2$) in the temperatures 700°–900°C, diffusion transformation at the temperatures above 650°C, which results in the Widmanstätten structures, and the isothermal conversion at a temperature below 650°C. The nucleation and growth of the γ_2 -phase may occur on the δ - γ phase grain boundary, or inside

the ferrite grains (Ref. 9). Nowacki and Lukojc (Ref. 9) showed that the main mechanism of secondary austenite precipitation is the diffusive transformation. An increase of the amount of γ_2 -phase in the HAZ was found to noticeably influence the joint hardness and corrosion resis-

tance. In particular, secondary austenite in DSSs promoted the loss of chemical balance between ferrite and austenite and the local decline of corrosion resistance of the alloy, particularly of the pitting corrosion. The authors reported that the microstructure of the specimens after post-

Table 1 — Chemical Composition of Base and Filler Material

Element	Chemical Composition (wt-%)	
	Base Material UNS S31808	Filler Material AWS ER2209
C	≤0.03	0.014
Cr	21–23	22.95
Ni	4.5–6.5	8.61
Mo	2.5–3.5	3.08
Mn	≤2.0	1.52
Si	≤1.0	0.47
N	0.15–0.20	0.163
P	≤0.03	0.015
S	≤0.02	0.0008
Cu	—	0.10

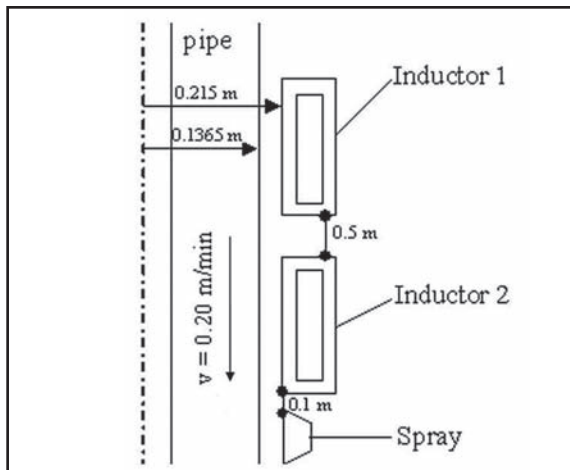


Fig. 3 — Schematic axisymmetrical view of the induction heat treatment.

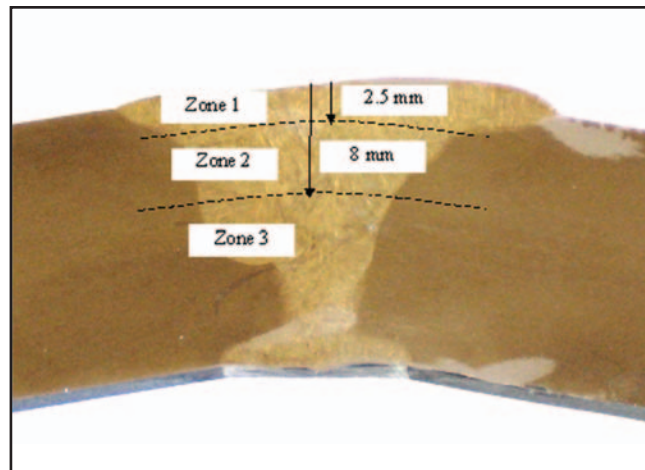


Fig. 4 — Macrograph of the joint and the marked zones under investigation.

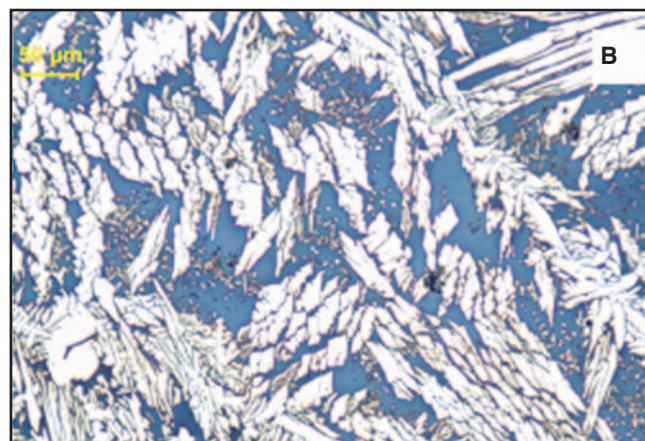


Fig. 5 — Micrographs of the FZ. A — Zone 1; B — Zone 3 (as-welded joint). Blue phase: ferrite; white phase: austenite; small white needles: secondary austenite.

weld heat treatment did not show intermediate phases as well as carbides and ni-

trides precipitates. J. O. Nilsson et al. (Ref. 10) showed that the secondary

Table 2 — Phase Proportion at Different Zones of the Bead (wt-%) (γ_2 : intragranular secondary Austenite) (The error ranges have been calculated for a confidence interval of 68.7%).

Zone	As-welded		Induction heat-treated	
	δ	γ_2	δ	γ_2
1	55.6±3.7	0	49.4±2.6	4.7±1.5
2	56.4±3.2	0	46.9±2.3	2.4±1.7
3	56.5±2.7	1.8±1.3	44.1±2.5	2.0±1.2

Table 3 — Chemical Composition of Primary and Secondary Austenite in FZ (wt-%) (The error ranges have been calculated for a confidence interval of 68.7%).

		As-welded		Heat-treated	
		γ	γ_2	γ	γ_2
Zone 1	Cr	23.3±0.1	—	22.9±0.3	21.5±0.1
	Mo	3.7±0.1	—	3.4±0.2	3.2±0.1
	Ni	8.1±0.1	—	8.4±0.1	9.7±0.1
Zone 3	Cr	23.3±0.2	22.0±0.1	22.9±0.1	21.9±0.1
	Mo	3.6±0.1	3.8±0.4	3.5±0.2	3.3±0.2
	Ni	6.6±0.3	7.1±0.1	7.6±0.1	8.7±0.1

austenite had lower concentrations of chromium, molybdenum, and nitrogen than the primary austenite. These observations were also confirmed by thermodynamic computer calculations, and the results were used to explain why secondary austenite is more susceptible to pitting attack than primary austenite. Garzón and Ramirez (Ref. 11) found a nonmonotonic relationship between the proportion of γ_2 and reheating temperature, a maximum γ_2 fraction being attained at ~1050°C. γ_2 formed at higher reheating temperatures (above ~1100°C) displayed an outer shell rich in chromium and nitrogen and a core region depleted in these alloying elements; in contrast, γ_2 formed at lower reheating temperature (below ~1000°C) showed a nearly homogeneous chemical composition.

It is hence clear that when PWHT is required, time and temperature must be controlled very accurately in order to preserve the corrosion resistance of the joints. However, to the authors' best knowledge, a satisfactory comprehension of the correlation between this property and PWHT

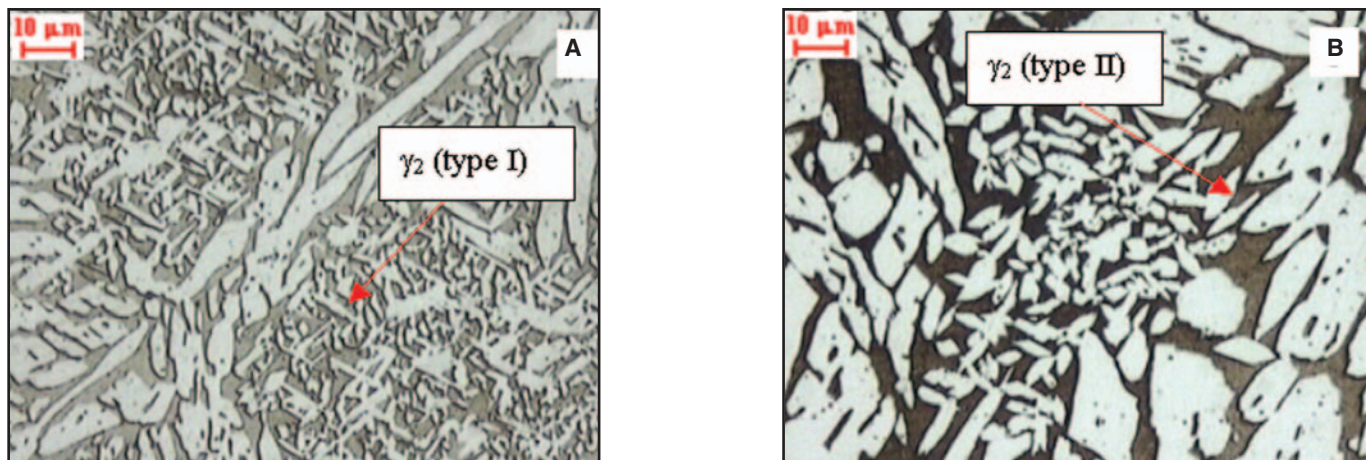


Fig. 6 — Micrographs of the FZ: A — Zone 1; B — Zone 3 (induction heat-treated sample). Dark phase: ferrite; white phase: austenite; small white needles: Widmanstätten-type secondary austenite (Types I and II).

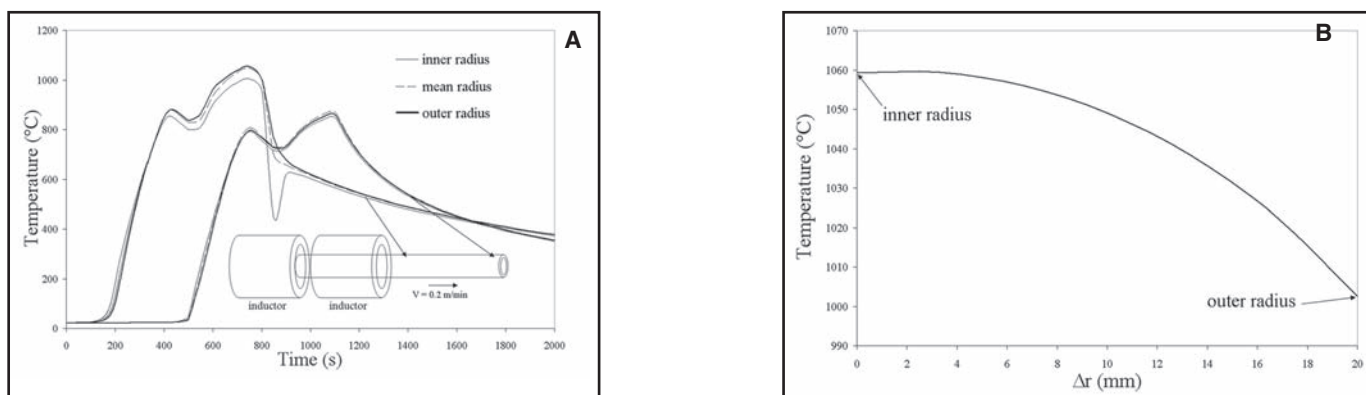


Fig. 7 — A — Time-temperature diagram; B — temperature profile across the thickness of the pipe at the time of highest reached temperatures.

process parameters is still not reached. Thus, the first objective of this work is to study in depth the correlation among microstructure, time, and temperature parameters, and corrosion resistance by means of several furnace postweld heat treatments. It was found that pitting corrosion resistance is affected by the presence of secondary austenite and its morphology, which in turn depends on time and temperature parameters.

Postweld heat treatment can be carried out by means of different technologies such as furnace, laser (Ref. 12), and induction heating. These last two technologies show the advantage of reducing the time cycle as compared to a furnace heat treatment; however, in these cases heating is not uniform through the thickness of the specimen, so that a different distribution of γ_2 fraction can be observed in the bead as compared to a homogeneous treatment.

The second aim of this work was thus the study of the influence of differently postweld heat treated samples of a DSS on corrosion resistance with particular attention to the comparison between induction and furnace heat treatment. If induction heat treatment is used, a temperature gradient is

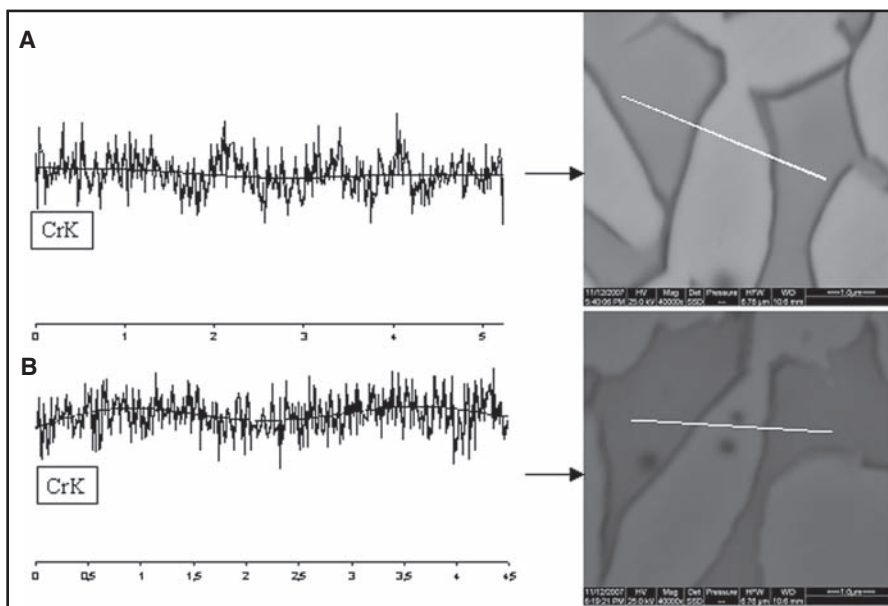


Fig. 8 — Line profiles across the secondary austenite. A — Zone 1; B — Zone 2.

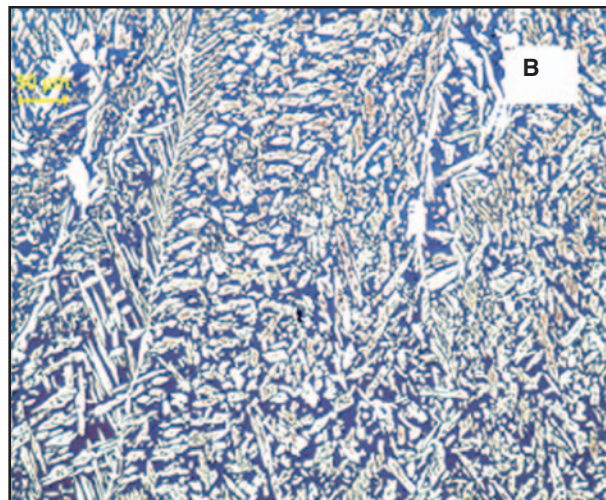
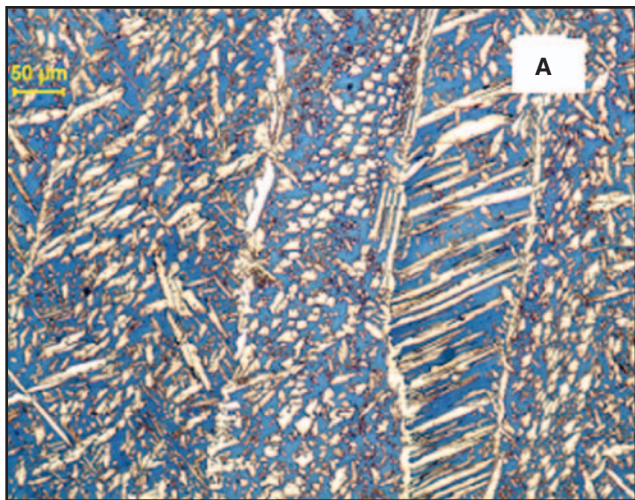


Fig. 9 — Micrographs of the FZ (Zone 1); furnace heat treatment (1100°C): A — 30 s; B — 600 s.

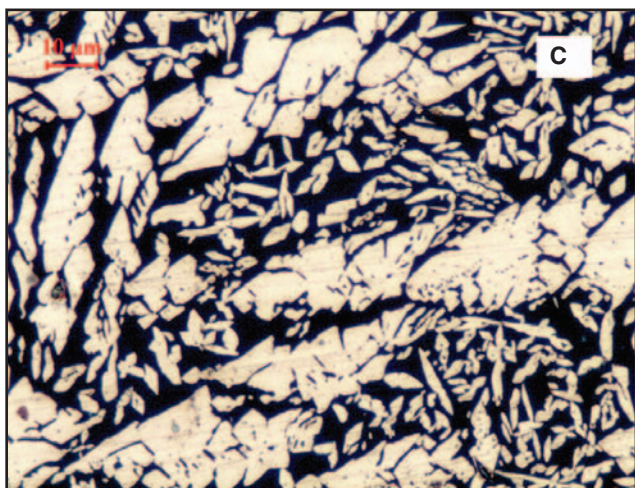
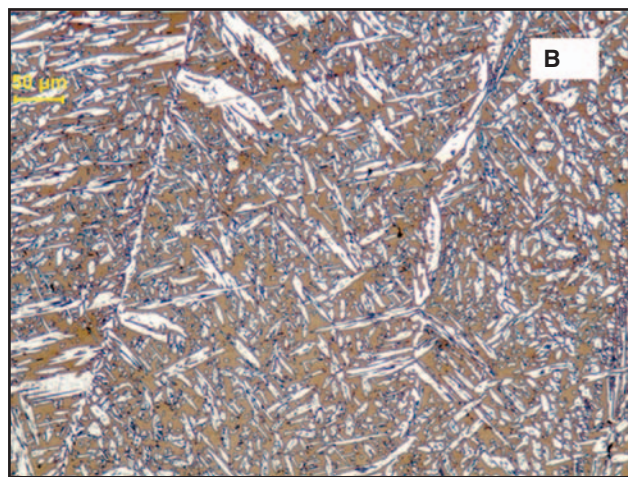
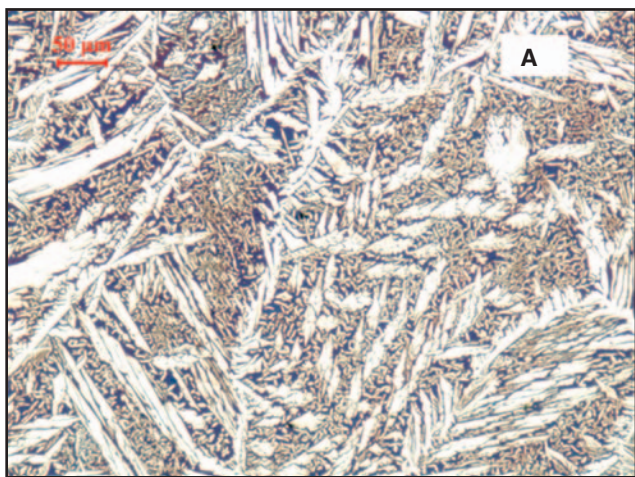


Fig. 10 — Micrographs of the FZ (Zone 1); furnace heat treatment (1050°C): A — 30 s; B — 600 s; C — 30 s.

established across the thickness of the workpiece, which influences the distribution and morphology of secondary austenite and thus the corrosion resistance of the joint.

taken from the production of pipes for oil industry applications. Some details about the groove adopted are shown in Fig. 2A. The chemical composition of the base

Materials and Methods

Materials and Welding Processes

The testing samples were extracted from two different weldments of UNS S31803 steel (also known as SAF 2205): a) longitudinally welded pipes, and b) butt-joint welds, which were respectively induction and furnace heat treated. A Sandvik 22.8.3.L AWS ER2209 wire was used as filler metal (AWS A5.9:ER 2209/EN 12072:22 9 3 N L standards). Such specimens have been

metal and the filler metal are reported in Table 1. Fusion zone (FZ) and HAZ were analyzed in the as-welded condition and after postweld heat treatment (Table 1). Seven welding runs were carried out for both joints. For operative reasons and in order to optimize the entire process, three different welding technologies were used. The first one was obtained by plasma arc welding (PAW), the second one by gas tungsten arc welding (GTAW), and the remaining runs by submerged arc welding (SAW). A schematic representation of the welding sequence is shown in Fig. 2B.

Microstructural and Corrosion Resistance Investigations

Microstructural investigations were carried out on specimens having similar process parameters and geometry to have comparable thermal field conditions. The effect of eventual variations in dilution ratios on the microstructure was not considered.

Microstructural investigations were executed by optical microscopy. Beraha's tint etch (20-mL HCl and 100-mL H₂O, 1-g

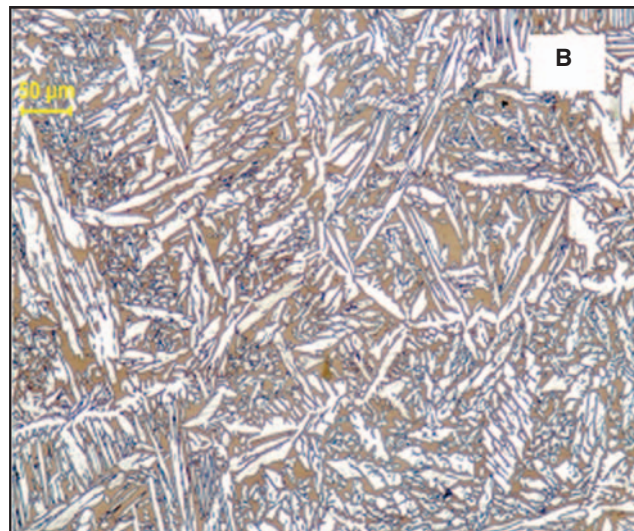
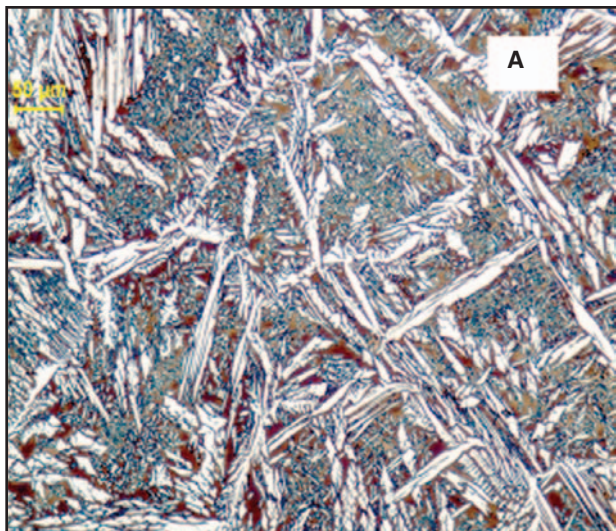


Fig. 11 — Micrographs (100×) of the FZ (Zone 1); furnace heat treatment (1000°C): A — 30 s; B — 600 s.

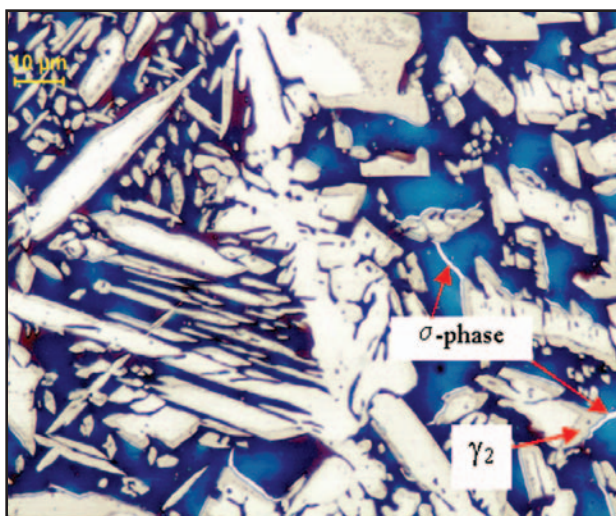


Fig. 12 — Micrographs of the FZ (Zone 1); furnace heat treatment (920°C), 600 s.

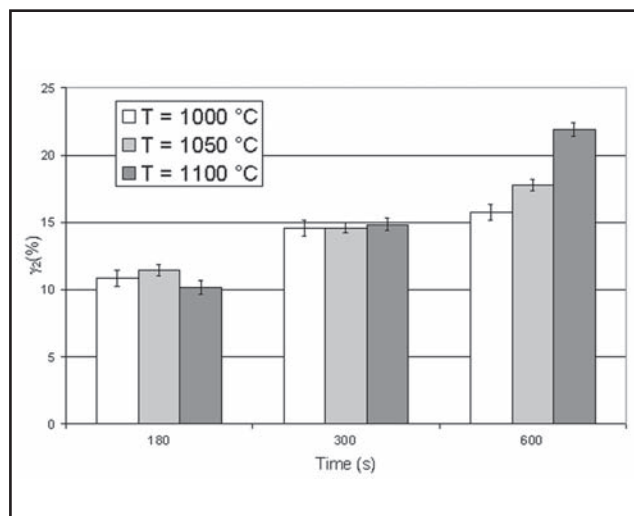


Fig. 13 — Total secondary austenite amount in Zone 1 of the bead as function of time and temperature of the postweld furnace heat treatment (the error bars have been calculated for a confidence interval of 68.7%).

K₂S₂O₅) was used to produce contrast between the primary phases (ferrite and austenite) and secondary γ ; finally, an electrolytic etch (50-g KOH, 100-mL H₂O, 2 V) was used to identify nonaustenitic secondary phases (σ , χ). A program for analyzing digital images (Leica Qwin) was used for the evaluation of the phases fraction. Each result was obtained by using the mean value of 16 fields of dimensions equal to 238 × 180 μ m. Detailed analyses of the microstructures and chemical compositions of the phases after different heat treatments were performed by environmental scanning electron microscopy (ESEM) combined with energy-dispersive microanalysis (EDS). A FEI Quanta 400 microscope equipped with EDAX Genesis 4000 Microprobe were used. Due to the tiny dimen-

sions of the phases, the microanalysis was carried out by using a spot size of 10 nm and long exposure times (about 5–7 min). The compositions of each analyzed phase was evaluated as the mean value of five different measurements.

Resistance to the pitting corrosion of the joints was evaluated according to ASTM G48 Method A. The specimens were dipped for 24 h in ferric chloride reagent (100-g FeCl₃ · 6H₂O in 900-mL H₂O) after being pickled for 5 min (20% HNO₃ + 5% HF, 60°C, 5 min). Exposure was initially performed at 22 ± 2°C (as prescribed in the previously mentioned standard); as the evidence of pitting corrosion was barely visible after etching at this temperature, other specimens were then etched at 30 ± 2°C in order to en-

hance the corrosion attack.

Induction Heat Treatment

As mentioned previously, the DSS pipes (having a diameter of 273 mm and thickness of 20 mm) were induction heated. To this purpose, two inductors of length 740 mm (28 coils) were used at a voltage of 663 V, a current of 1000 A, and a frequency of 469 Hz. The pipe was fed into the inductor coils at a speed of 0.20 m/min. A nozzle close to the coils' end sprayed water onto the steel pipe in order to quench it immediately after leaving the heating section. Figure 3 shows a schematic view of the experimental setup.

In order to simulate the thermal field generated by induction in the workpiece,

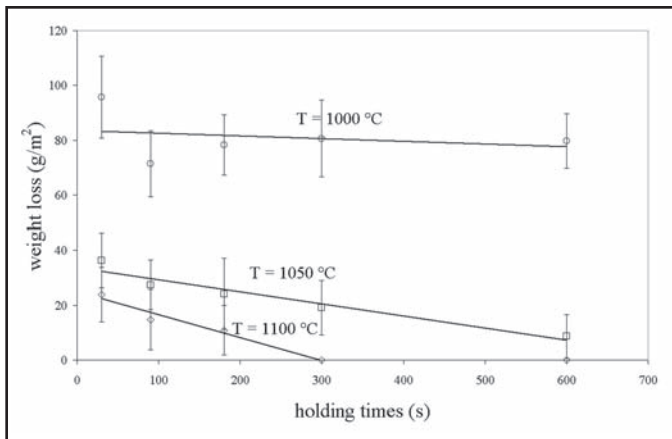


Fig. 14 — Weight loss as a function of the holding time and temperature of the furnace heat treatment (temperature of the test corrosion: 30°C) (the error bars have been calculated for a confidence interval of 68.7%).

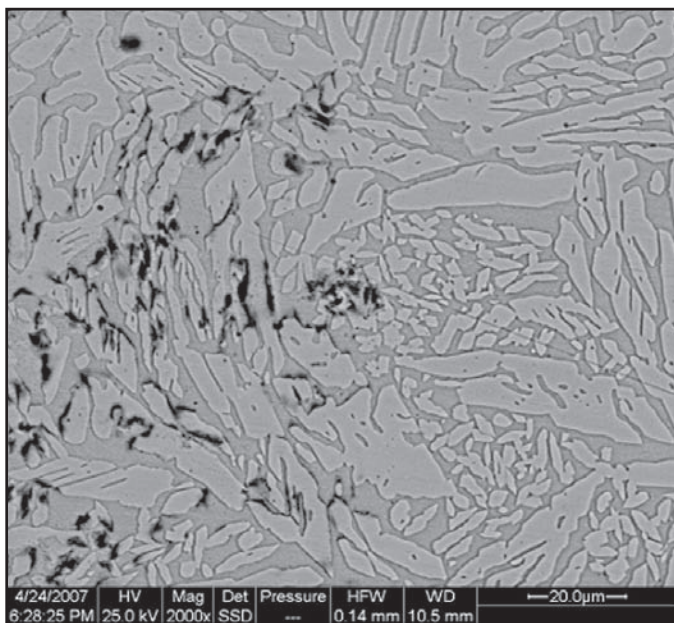


Fig. 15 — ESEM micrograph of FZ of the induction heat-treated sample after test corrosion at $T=30^{\circ}\text{C}$, 4 h.

a numerical analysis was carried out by using the Sysweld 2006.1® code.

Furnace Heat Treatment

The furnace heat treatments were carried out using laboratory furnaces on samples obtained from a butt joint (sheet thickness: 20 mm) welded with the same parameters used for the pipes. In order to find the best process parameters, several annealing treatments were performed at various temperatures (920°, 1000°, 1050°, 1100°C) and with different time intervals (30, 90, 180, 300, 600 s). The heating rates from ambient temperature to each annealing temperature (920°, 1000°, 1050°,

and 1100°C) were monitored by measuring the core and skin temperatures of the workpiece with two thermocouples.

Results and Discussion

As-Welded Specimens

Figure 4 shows a typical cross section of a weld where the locations for the extraction of the specimens used for investigation are marked.

The FZ of the as-welded joint was characterized by a ferrite/austenite ratio of 57%/43%. However, some microstructural distinctions among the different zones of the bead can be observed — Fig. 5. For example, secondary austenite was found chiefly in those zones that were subjected to repeated thermal cycles induced by multipass welding (i.e., Zone 3, Fig. 5B), as compared to the portion of the bead welded on the last run (i.e., Zone 1, Fig. 5A). No other secondary phases were detected in

FZ and HAZ.

Induction Heat Treated Specimens

The micrographs of the induction heat treated specimens (Fig. 6) showed the presence of secondary austenite in the whole bead. However, considering in this calculation only the γ_2 precipitated into the δ -grains (intragranular secondary austenite), the fraction of secondary austenite was found to vary along the bead. Higher fractions of γ_2 were detected near to the weld bead surface (Zone 1) than in the inner zones. Nevertheless, the total amount of austenite ($\gamma + \gamma_2$) was larger in Zone 3 than in Zones 1 and 2. Table 2 summarizes the

collected results. From a general viewpoint, a good balance between austenite and ferrite was achieved (56.6% (γ) to 43.4% (δ)).

According to the classification given by Nowacki and Lukojc (Ref. 13), two kinds of secondary austenite were observed both in the induction and furnace heat treated samples: thin Widmanstätten-type needles (called in this work ' γ_2 -Type I') and coarse Widmanstätten-type needles (called ' γ_2 -Type II'), as shown in Fig. 6. Moreover, secondary austenite in Zone 3 of the bead is coarse (γ_2 -Type II), whereas the secondary austenite in Zone 1 (γ_2 -Type I) exhibits a fine morphology.

The EDS microanalysis showed that the secondary austenite γ_2 contains different amounts of Cr, Mo, Ni compared to the primary austenite. Results are listed in Table 3. Generally, as confirmed by other authors (Refs. 9, 10, 14), it was found that the secondary austenite is depleted in α -stabilizing elements and richer in γ -stabilizing elements.

The induction heat treatment of a pipe (set 2.5 m long) was simulated by means of a finite element (FE) calculation method. Due to the axisymmetrical conditions, only a half section of the whole geometry was modeled. To model the pipe, 960 isoparametric rectangular elements (with four nodes) were used. Thermal and magnetic properties of the material under investigation were taken from the literature (Refs. 15, 16), likewise the properties of the cooling medium and the inductors (copper). Finally, a magnetic-thermic coupled analysis was carried out following the routine described by Magnabosco et al. (Ref. 17). The results of the numerical simulation are shown in Fig. 7. It was found that the highest temperatures were reached at the inner radius of the pipe (1060°C) with a temperature gap (ΔT) of about 50°–60°C between the inner and outer radius.

The lowest temperatures (between 1000° and 1020°C) were reached at the outer surface of the pipe, thus along the head of the bead (Zone 1); this could explain the greater fraction of small γ_2 -particles (Type I) precipitated there. On the opposite, as the inner surface of the pipe faced the highest temperatures (1050°–1060°C), it can be expected that the bead bottom (Zone 3) is characterized by low fraction of intragranular Type I secondary-austenite and a general coalescence process of the secondary austenite laths (evolution from the Type I to Type II morphology). Besides, further secondary austenite nucleated and grew at the grain boundary of the primary phase.

The line-scan analysis across the δ/γ_2 interface (Fig. 8) showed that at lower temperature (about 1000°C) a homogeneous composition characterizes the two

phases, whereas at higher temperature a slight chromium segregation developed in the outer shell of γ_2 phase. Such results are in agreement with those obtained by Garzón and Ramirez (Ref. 11).

The induction heat-treated specimens showed good corrosion resistance at 22°C; however, each of them displayed some pitting in the outer surface of the pipe at 30°C. In particular, a mean weight loss of 128 g/m² was found. Since pitting corrosion nucleated at the interface δ/γ , this behavior can be correlated to the higher amount of grain boundaries induced by secondary austenite (Type I) at the head of the bead compared to the inner zones (Table 2).

Due to the low atomic mass, it was not possible to detect the nitrogen content. However, by using the thermodynamic data obtained by Nilsson et al. (Ref. 10), it was possible to estimate the PREN (pitting resistance equivalent number = %Cr + 3.3%Mo + 16%N) (Ref. 4) at the different zones of the bead. In particular, it was found by using the Thermo-Calc program and supposing a thermodynamic equilibrium between ferrite and austenite was reached at 1300°C that the nitrogen content decreased from 0.55 wt-% at 1300°C to 0.14 wt-% at 900°C (with an intermediate value of about 0.18 wt-% at 1000°C).

Coupling these data with the experimental values (Table 3), the PREN value of γ_2 near the upper surface of the bead was found at about 33 (against a value of about 38 of the primary austenite).

As concluded by Nilsson et al., the sensibility of the secondary austenite to the pitting corrosion can thus be explained with the minor Cr-Mo-N concentration; however, this conclusion is not sufficient to explain why the zones where secondary austenite of Type I precipitated were characterized by lower corrosion resistance.

Furnace Heat-Treated Specimens

The furnace heat-treated specimens showed a homogeneous microstructure in the whole bead due to a more uniform temperature distribution across the thickness of the weld. The secondary austenite needles appear initially fine (i.e., Type I) and then tend to coarsen with increased annealing time. This microstructural evolution is more substantial at increased times and temperatures of the heat treatment (Figs. 9–11). The micrograph of Fig. 10C shows, in particular, a magnification (500×) of the finer microstructure of a sample annealed for 30 s.

Further, the presence of the harmful σ phase was encountered in samples held at 920°C for times exceeding 300 s (Fig. 12). In fact, when the DSS is annealed in the temperature range between 650° and 950°C, α phase can form after relatively

long holding times, as the eutectoid reaction $\delta \rightarrow \gamma_2 + \sigma$ takes place. The precipitation rate of σ phase is maximum for isothermal aging carried out at a temperature around 850°C. The higher the aging temperature, the coarser are the sigma precipitates (Refs. 18, 19). In particular, it was detected on the base metal a σ phase fraction of about 2 wt-% after aging for 5 min at 850°C (Ref. 20). The α/σ or γ/σ phase boundary acts as an initiation site for the metastable pitting because of the depletion of Cr and Mo around the σ phase (Ref. 5).

The fraction of total secondary austenite was obtained by analyzing the digital micrographs taken on eight samples, each characteristic for a different heat treatment condition (temperature and time). The amount of total secondary austenite (i.e., both isolated and co-precipitated γ_2) was calculated as the difference between the fractions of austenites of the specimen in the as-welded condition (showing only primary austenite) and after heat treatment. The results are summarized in Fig. 13.

Figure 13 shows the increment of secondary austenite precipitation with the annealing time. Furthermore, it is shown that after 300 s the higher annealing temperature causes a more extensive volume increment of γ_2 .

The corrosion tests have shown an increment of the pitting corrosion resistance at increasing holding times. The best results were found at 1100°C, as shown in Fig. 14.

It was observed (Fig. 15) that corrosion started at the interface between ferrite and both secondary austenite precipitated at the grain boundary of primary austenite and the γ_2 precipitated into the ferrite grains.

The different pitting corrosion resistances of the furnace heat-treated specimens can be interpreted in terms of secondary austenite precipitation. In fact, γ_2 is less resistant to pitting corrosion compared to other phases (PREN(γ_2) = 33, PREN(γ) = 38) and introduces in the material new grain boundaries that are preferential nucleation sites for the chemical etching. These grain boundaries decrease with the increase in temperature and time of the heat treatment. Thus, it was found that pitting corrosion is influenced not only by the depleted amount of Cr-Mo-N in γ_2 compared to the primary austenite composition (as found in previous works (Ref. 10)), but also by the amount of δ/γ_2 interfaces that are favorable sites for pitting nucleation.

The presence of intragranular chromium nitrides in heat-treated welded specimens was not detected by using light microscope (LOM) or ESEM. This seems in agreement with Ref. 21, in which it is shown that after the early stages of the re-

heating (10 s at 1000°–1100°C) most of such precipitation dissolves. That work proposes that N enrichment of ferrite as a result of nitride dissolution promotes secondary austenite precipitation; moreover, a heterogeneous nucleation of intragranular austenite on the intragranular nitrides is proposed. In any case, such chromium nitrides are not seen after heat treatments longer than 10 s, so that their influence on corrosion properties of heat-treated specimens is disregarded in this work.

The different types of secondary austenite across the thickness of the induction heat-treated specimens, where a great amount of secondary austenite of Type I was observed near the head of the bead, may explain the reduction of pitting corrosion resistance in that zone. Finally, the as-welded samples showed better pitting corrosion resistance compared to the induction heat-treated ones. This behavior can be attributed to the absence of secondary austenite in the as-welded samples and thus a minor amount of pitting nucleation sites. Following the experimental results obtained in this work, better corrosion resistance of the induction heat-treated pipes may be obtained by modifying the process parameters, aiming to reach higher annealing temperatures at both sides of the bead (e.g., about 1100°C on the bottom side and about 1050°C at the head).

Conclusions

This work studied the influence of postweld heat treatments on the corrosion resistance of a duplex stainless steel SAF 2205 and the comparison between postweld induction heat treatment and conventional furnace heat treatment.

The main results of the experimental investigations are as follows:

a) As a result of metallographic investigations of FZ after postweld annealing, three phases were observed: primary ferrite (δ), primary austenite (γ), and secondary austenite (γ_2). The postweld heat treatment of duplex stainless steels contributes to the creation of secondary (γ_2) austenite.

b) The induction heat-treated specimens showed a different morphology of secondary austenite across the section of the FZ (thin Widmanstätten-type needles (' γ_2 -Type I') and coarse Widmanstätten-type needles (' γ_2 -Type II')) with a prevalence of γ_2 (Type I) in the outer surface of the pipe. This was attributed to the lower temperature reached in that zone compared to the one reached near the inner radius of the workpiece.

c) The furnace heat treatment showed that secondary austenite evolves from Type I to Type II according to time and temperature. The higher the temperature,

the faster and higher the pitting corrosion resistance reached by the specimens. A rationale of this behavior could be the evolution of the morphology of secondary austenite from Type I to Type II with a following reduction of the δ/γ_2 interface, where pitting corrosion generally starts.

These results, together with the calculated temperature distribution in the induction heat-treated specimens, explain the low pitting corrosion resistance found near the outer radius of the pipes and the better chemical properties of the as-welded samples. Better results can be reached by increasing and adjusting the temperature across the thickness of the pipe by modifying the process parameters such as frequency, voltage, speed, or inductor length.

The final outcomes of the work are consequently:

1) The corrosion properties in postweld heat-treated duplex stainless steel SAF 2205 are related not only to the presence of the secondary austenite but also to its morphology, which in turn depends on the heat treatment parameters: a coarse secondary austenite induces better corrosion properties compared to the finer one.

2) If induction heat treatment is carried out, a significant thermal gradient may arise across the thickness of the weld so that, according to the results of point 1, different corrosion properties may be found across the thickness of the joint.

Acknowledgments

The authors gratefully acknowledge the technical support of Giacomo Mazzacavallo and Enrico Della Rovere, technicians of the metallurgical laboratory of DTG – University of Padova.

References

1. Kobayashi, D. Y., and Wolyne, S. 1999. Evaluation of the low corrosion resistant phase formed during the sigma phase precipitation in duplex-stainless steels. *Materials Research* 2(4): 239-s to 247-s.
2. Kordatos, J. D., Fourlaris, G., and Papadimitriou, G. 2001. The effect of cooling rate on the mechanical and corrosion properties of SAF 2205 (UNS 31803) duplex stainless steel welds. *Scripta Materialia* 4(3): 401-s to 408-s.
3. Bonollo, F., Tiziani, A., and Ferro, P. 2005. Microstructural evolution of duplex and superduplex stainless steels in relation to welding processes. *La Metallurgia Italiana* 97(2): 27-s to 38-s.
4. Lopez, N., Cid, M., and Puiggali, M. 1999. Influence of σ -phase on mechanical properties and corrosion resistance of duplex stainless steels. *Corrosion Science* 41: 1615-s to 1631-s.
5. Park, C. J., Shankar Rao, V., and Kwon, H. S. 2005. Effects of sigma phase on the initiation and propagation of pitting corrosion of duplex stainless steel. *Corrosion* 61: 76-s to 83-s.
6. ASTM A928 / A928M -08a, *Standard Specification for Ferritic/Austenitic (Duplex) Stainless Steel Pipe Electric Fusion Welded with Addition of Filler Metal* (www.astm.org/Standards/A928.htm).
7. Young, M. C., Tsay, L. W., Shin, C.-S., and Chan, S. L. I. 2007. The effect of short time heat treatment on the fatigue crack growth of 2205 duplex stainless steel welds. *International Journal of Fatigue* 29(12): 2115-s to 2162-s.
8. Melotti, G., Bertelli, R., Zanenco, M., Calliari, I., and Ramous, E. 2005. Solution treatment in duplex stainless steels. *La Metallurgia Italiana* 4: 39-s to 42-s.
9. Nowacki, J., and Lukojc, A. 2005. Structure and properties of the heat-affected zone of duplex steels welded joints. *Journal of Materials Processing Technology* 164(165): 1074-s to 1081-s.
10. Nilsson, J. O., Karlsson, L., and Andersson, J.-O. 1995. Secondary austenite formation and its relation to pitting corrosion in duplex stainless steel weld metal. *Mater. Sci. Tech.* 11: 276-s to 283-s.
11. Garzón, C. M., and Ramirez, A. J. 2006.

Growth kinetics of secondary austenite in the welding microstructure of a UNS S32304 duplex stainless steel. *Acta Materialia* 54(12): 3321-s to 3331-s.

12. Capello, E., Castelnuovo, M., Previtali, B., and Vedani, M. 2005. Laser welding and heat treatment of duplex stainless steels. *La Metallurgia Italiana* 2: 9-s to 14-s.

13. Nowacki, J., and Lukojc, A. 2006. Microstructural transformations of heat affected zones in duplex steel welded joints. *Materials Characterization* 56(4-5): 436-s to 441-s.

14. Karlsson, L., and Pak, S. 1991. Welding of duplex stainless steels - Properties of SMAW-, FCAW-, and SAW-welded joints. *Proc. 'Stainless Steels 91'*, Chiba, Japan, The Iron and Steel Institute of Japan, 2, p. 1101-1108.

15. Mészáros, I. 2006. Magnetic characterization of duplex stainless steel. *Physica B* 372(1-2): 181-s to 184-s.

16. Tavares, S. S. M., da Silva, M. R., and Neto, J. M. 2000. Magnetic property changes during embrittlement of a duplex stainless steel. *Journal of Alloys and Compounds* 313(1-2): 168-s to 173-s.

17. Magnabosco, I., Ferro, P., Tiziani, A., and Bonollo, F. 2006. Induction heat treatment of a ISO C45 steel bar: Experimental and numerical analysis. *Computational Materials Science* 35(2): 98-s to 106-s.

18. Sieurin, H., and Sandström, R. 2007. Sigma phase precipitation in duplex stainless steel 2205. *Mater. Sci. Eng. A* 444(1-2): 271-s to 276-s.

19. Huang, C.-S., and Shih, C.-C. 2005. Effects of nitrogen and high temperature aging on phase precipitation of duplex stainless steel. *Mater. Sci. Eng. A* 402(1-2): 66-s to 75-s.

20. Ferro, P., Cervo, R., Bonollo, F., and Bertelli, R. 2007. Setup and implementation of a numerical model for the simulation of heat treatment of duplex stainless steels. *Proc. International Conference Duplex 2007*. Grado, Italy.

21. Ramirez, A. J., Brandi, S. D., and Lippold, J. C. 2004. Secondary austenite and chromium nitride precipitation in simulated heat affected zones of duplex stainless steels. *Science and Technology of Welding and Joining* 9(4): 301-s to 313-s.

Call for Papers

15th Int'l Conf. on the Joining of Material

The 15th International Conference on the Joining of Materials (JOM-15) and the 6th International Conference on Education in Welding (ICEW-6) Conference and Exhibition organized by JOM Institute and supported by Dansk Metal, Danish Welding Society, and DSL FORCE Technology, will be held May 3-6, 2009, Helsingør, Denmark.

A full technical program on welding technology and education and training will be conducted. The main topics are listed below.

1) Recent developments in joining technology — welding, soldering, brazing, and projects, with the emphasis on industrial applications,

2) Welding quality — properties and environmental considerations,

3) Welding management and qualification of welding personnel.

The organizers cordially invite you to send a title of your presentation and a short abstract by December 31, 2008. Notification of acceptance and author's guidelines will follow after review of the abstracts. Full papers must be received by March 2009. Please send your name, address, title, and abstract to: Alan Parnes (Dansk Metal). e-mail alan.parnes@danskmetal.dk. For further information about the conference contact JOM. Gilleleje Strandvej, 28. DK-3250 Gilleleje. Denmark. Telephone: +45 48355458, e-mail jom_aws@post10.tele.dk.